

VWA3A-derived ependyma promoter drives increased therapeutic protein secretion into the CSF

Ellie M. Carrell,¹ Yong Hong Chen,¹ Paul T. Ranum,¹ Stephanie L. Coffin,¹ Larry N. Singh,² Luis Tecedor,¹ Megan S. Keiser,¹ Eloise Hudry,³ Bradley T. Hyman,^{3,4,5} and Beverly L. Davidson^{1,6}

¹Raymond G. Perelman Center for Cellular and Molecular Therapeutics, The Children's Hospital of Philadelphia, Philadelphia, PA 19104, USA; ²Center for Mitochondrial and Epigenomic Medicine, The Children's Hospital of Philadelphia, Philadelphia, PA 19104, USA; ³Department of Neurology, Massachusetts General Hospital, Boston, MA 02114, USA; ⁴Massachusetts Alzheimer's Disease Research Center, Charlestown, MA 02129, USA; ⁵Harvard Medical School, Boston, MA 02115, USA; ⁶Department of Pathology & Laboratory Medicine, University of Pennsylvania, Philadelphia, PA 19104, USA

Recombinant adeno-associated viral vectors (rAAVs) are a promising strategy to treat neurodegenerative diseases because of their ability to infect non-dividing cells and confer long-term transgene expression. Despite an ever-growing library of capsid variants, widespread delivery of AAVs in the adult central nervous system remains a challenge. We have previously demonstrated successful distribution of secreted proteins by infection of the ependyma, a layer of post-mitotic epithelial cells lining the ventricles of the brain and central column of the spinal cord, and subsequent protein delivery via the cerebrospinal fluid (CSF). Here we define a functional ependyma promoter to enhance expression from this cell type. Using RNA sequencing on human autopsy samples, we identified disease- and age-independent ependyma gene signatures. Associated promoters were cloned and screened as libraries in mouse and rhesus macaque to reveal cross-species function of a human DNA-derived von Willebrand factor domain containing 3A (VWA3A) promoter. When tested in mice, our VWA3A promoter drove strong, ependyma-localized expression of eGFP and increased secreted ApoE protein levels in the CSF by 2–12× over the ubiquitous iCAG promoter.

INTRODUCTION

Adeno-associated viruses (AAVs) are small, non-pathogenic viruses that can be engineered to deliver DNA to target cells. They have been used extensively for research as well as preclinical and clinical applications for their ability to infect non-dividing cells and confer long-term transgene expression. Cellular targeting is mediated by the capsid, of which there are 12 parent serotypes with over 150 naturally occurring variants, as well as a growing list of laboratory-modified variants that alter parent tropism. Further specificity can be conferred by inclusion of cell-type-specific promoters,^{1–3} enhancers,^{4–7} or microRNA target sites^{8,9}; however, translation of these elements may be hindered due to limited conservation between experimental models and humans.¹⁰

Despite the large number of available capsid types, widespread delivery to the brain and spinal cord remains a challenge in adolescents and adults. Systemic administration of naturally occurring AAV9 is commonly used for broad central nervous system (CNS) targeting for its ability to cross the blood-brain barrier (BBB). Interestingly, however, AAV9 tropism changes with age at administration and exhibits limited neuronal targeting in adult primates,¹¹ a drawback for application in treating neurodegenerative disorders with onset years to decades after birth. Capsid evolution of AAV9 has identified multiple variants with improved neuronal tropism and reduced peripheral off-targeting; however, systemic doses remain high and broad species compatibility has not been validated.^{12–16}

Alternatively, CNS transduction can be achieved with lower doses of AAV delivered to the cerebrospinal fluid (CSF) via intracerebroventricular (i.c.v.), intra-cisterna magna, and lumbar puncture infusion.^{17–21} These direct approaches obviate the need for capsids that can cross the BBB and have thus utilized multiple different serotypes.²² One disadvantage to this approach is frequent toxicity in dorsal root ganglion (DRG) sensory neurons.^{23,24} In a large meta-analysis, 83% of non-human primate (NHP) subjects administered AAV via CSF had detectable lesions that were independent of capsid type or transgene promoter (ubiquitous or neuron specific) and were consistent at all levels of CNS injection.²² De-targeting expression in DRG neurons using a miRNA binding site eliminated toxicity while maintaining expression in relevant brain regions,⁸ supporting further development of DRG exclusive transgenes.

For broad CNS delivery of secreted proteins, we and others have taken advantage of the ability for certain CSF-delivered AAVs to specifically

Received 14 April 2023; accepted 12 July 2023;
<https://doi.org/10.1016/j.omtn.2023.07.016>

Correspondence: Beverly L. Davidson, Raymond G. Perelman Center for Cellular and Molecular Therapeutics, The Children's Hospital of Philadelphia, Philadelphia, PA 19104, USA.

E-mail: davidsonbl@chop.edu



Table 1. Patient information

Patient ID	Age at death (years)	Sex	Clinical diagnosis
1906	71	male	control
1907	≥ 90	female	AD
1932	63	male	HD
1911	41	male	control
1930	81	male	FTD
1939	75	male	LBD
1940	77	female	dementia
1943	82	male	LBD
1946	88	male	control

AD, Alzheimer's disease; HD, Huntington's disease; FTD, frontotemporal dementia; LBD, Lewy body dementia.

transduce ependymal cells that line the walls of the brain ventricles and central canal of the spinal cord.^{25–28} Specific transduction can be achieved by i.c.v. delivery of AAV4 in mice and AAV2 in rhesus macaque (unpublished results).^{27,29} Ependyma cell cilia control CSF flow throughout the ventricles and the CNS, and a subpopulation of specialized ependymal cells forms the choroid plexus, the site of CSF production. Importantly, their position at the ventricle margin enables widespread delivery of secreted therapeutic protein throughout the brain via ventricular, subarachnoid, and perivascular spaces while avoiding potentially toxic direct neuronal expression.^{22,26,30,31} Moreover, ependyma cells are known to be post-mitotic, unlike those in the subependymal stem cell compartments.³² Application of this approach using ubiquitous transgene promoters has enabled clinically relevant protein delivery throughout the brain in mice^{27,33} and dogs.²⁶

Here, we sought to improve the safety and durability of this strategy by identifying promoter elements for ependyma-specific transgene expression. To ensure functional use of regulatory sequences in a setting of disease, candidate genes and their associated promoters were defined by a cohort of healthy and clinically diagnosed neurodegenerative disease patients. Barcoded human promoter AAV libraries were delivered to both mouse and rhesus macaque to identify cross-species function of a human *VWA3A* promoter for robust expression and secretion of therapeutic protein into the CSF.

RESULTS

Identification and validation of ependyma-enriched genes

To identify genes with strong, consistent expression in ependyma regardless of age or disease state, we obtained samples from nine post-mortem brains aged 41–90 years with and without clinically diagnosed neurological disorders (Table 1). Each patient set was comprised of paired white matter and/or gray matter samples, one at the ventricle margin containing the ependyma, the other in the adjacent parenchyma (Figure 1A). Ependyma-enriched genes were identified computationally as genes showing increased expression in ependyma-containing samples over those without. We identified a to-

tal of 608 specific ependyma-enriched genes in Control and 1,857 genes in Disease groups, with 349 found in both groups (Figure 1B). Overlapping hits were filtered to exclude transcripts without a mouse homolog, low abundance in either group, as well as those with a relative abundance ratio between Disease and Control groups of less than 0.5. Remaining genes were ranked on expression in the Disease group (Table S1). Top hits included *FOXJ1*, a known regulator of cilia development, *RGS1*, an attenuator of G-protein signaling, *ODF3B*, a protein of respiratory and fallopian cilia, as well as genes with limited characterization such as *VWA3A*. Hits were confirmed against published RNA-ISH data from the Allen Brain Atlas for specificity in the brain region of interest.

Definition of ependyma promoters and library screening

For functional application in mice, we used the UCSC Genome Browser to identify promoter-like signatures within 3,000 bp upstream of the transcriptional start site of top genes. Signatures included histone methylation (HEK4me1, H3K4me3), histone acetylation (H3K27Ac), DNase I hypersensitivity, and dense transcription factor binding sites. These regions were PCR amplified and placed upstream of an eGFP reporter (Figure 1C). Select promoters (*FoxJ1*, *Odf3b*, and *Vwa3a*) were packaged individually into AAV4 capsids and delivered by i.c.v. injection into adult wild-type (WT) mice. After 4 weeks, sectioned tissues revealed strong, ependyma-localized expression of eGFP, higher than observed for the ubiquitous CMV promoter (Figure 1D).

Tissue-specific transcriptional regulation is poorly conserved among species,¹⁰ therefore regulatory sequences verified in mouse will not necessarily function in humans or NHPs. As such, we isolated putative promoter sequences from human DNA using the same criteria as in mouse and placed them upstream of an eGFP reporter. For library screening, we appended a unique 3 bp DNA barcode in the 3' UTR of the transgene (Figure 2A). A variant containing the ubiquitous iCAG promoter and one containing no promoter sequence (None) were included as positive and negative controls, respectively. Plasmids were pooled and generated as a single-vector library, packaged in either AAV2 for NHP or AAV4 for mouse (Figure 2B).

The AAV4 library was delivered by i.c.v. injection into adult WT mice at 1E10, 5E10, or 1E11 viral genomes (vg) per animal. After 3 weeks, ependyma was micro-dissected from ice-cold brain slabs. RNA was isolated and targeted amplicon sequencing at the 3 bp barcode was used to measure relative transcription downstream the human-derived promoters. Two low-dose (1E10 vg) samples had inadequate amplification for analysis. Among those sequenced, barcode distribution was similar among all samples at all doses (Figure 2C), with relative enrichment of transcripts driven by our positive iCAG control and a promoter derived from the human von Willebrand factor domain containing 3A (*VWA3A*) gene (Figure 2D).

A similar AAV2 library was delivered to two adult rhesus macaques at a dose of 2E13 vg/animal. After 3 weeks the brains were harvested, and ependyma was micro-dissected from the ventricle and spinal

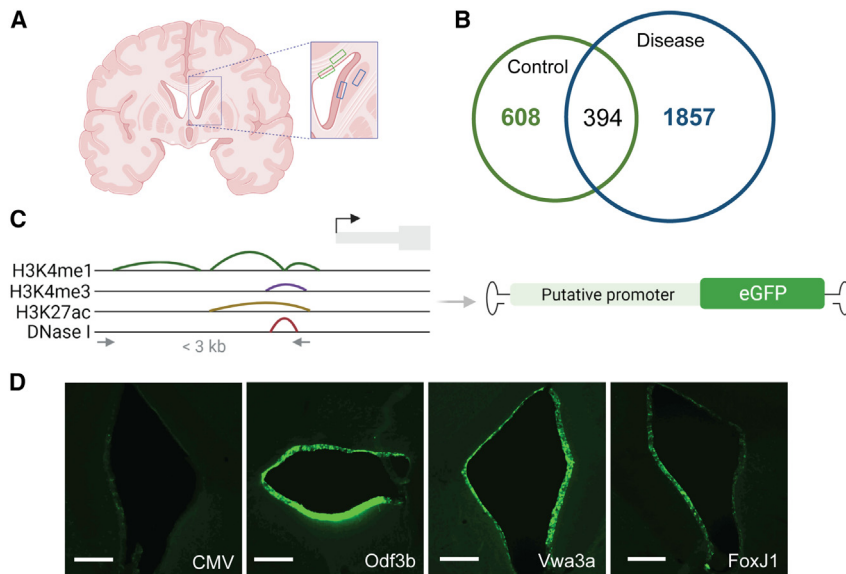


Figure 1. Patient sample isolation and identification of ependyma-specific gene signatures

(A) Cartoon depicting the location of four samples obtained from each patient. Each set contained two white matter and two gray matter samples, one at the ventricle margin containing ependyma, the other in the adjacent parenchyma. (B) Venn diagram highlighting ependyma-enriched genes in Control and Disease groups. (C) Genetic signatures used to define potential promoter regions. (D) Representative images of AAV4 with eGFP expression downstream of the ubiquitous CMV or mouse-derived ependyma promoters following i.c.v. injection. Mice were injected with varying doses with CMV matching the highest dose (see [materials and methods](#)). Scale bars, 250 μ m.

column margins. Targeted RNA sequencing revealed similar promoter use-distribution among the two animals that varied by location ([Figure 2E](#)). Barcodes could only be amplified from the spinal column of one subject. When normalized to virus input, iCAG showed the highest enrichment in all areas, followed by *VWA3A* and *FOS*, specifically in the lateral ventricles ([Figure 2F](#)).

Modification of promoters to include introns for potential intron-mediated enhancement

We next took a subset of human promoters (*CD42A*, *VWA3A*, *OGFRL1*, *ANXA1*, *ANXA2*, and *FOS*) and incorporated a short (133 bp) or long (951 bp) intron with the goal of increasing expression through intron-mediated enhancement (IME).³⁴ At this time eGFP reporters were also exchanged for APOE2, a variant of APOE that is negatively associated with the development of Alzheimer's disease (AD) and previously shown to reduce amyloid plaques in existing disease models ([Figure 3A](#)).^{33,35} Despite our selection criteria that limited brain expression to ependymal cells, HEK293 cells could express our variants, enabling screening of splicing and protein translation. Individual variants were transfected into HEK293 cells and harvested at 24 h. RNA (R) splicing was assessed by PCR across the intron and compared with amplified plasmid DNA (D), represented as unspliced ([Figure S1A](#)). All short and long introns were efficiently spliced, except for the short intron from the *ANXA1* variant. As APOE2 is a secreted protein, we measured APOE2 protein in cell lysates and media. When compared with the complementary "No intron" or original variant, inclusion of an intron generally increased protein expression, with the longer intron producing greater levels than the short intron ([Figures S1B](#) and [S1C](#)). Overall expression was variable among the promoters, with *FOS* yielding relatively high protein output compared with other promoters. This finding is consistent with *FOS* being highly expressed in non-brain tissues, including kidney.

A library of 18 intron-containing and original parent variants were packaged in AAV2 and delivered at a dose of 2.8E13 vg via i.c.v. delivery to two adult rhesus macaques. After 4 weeks, the brains and spinal columns were harvested and the ependyma was micro-dissected for RNA isolation and barcode analysis. As observed in our initial NHP experiment, promoter use was consistent among animals, with variations observed within single animals at different anatomical locations (see, for example, *FOS* and *VWA3A*; [Figure 3B](#)). Interestingly, despite only having one usable spinal column sample from this and our prior experiment, *ANXA2* showed consistent enrichment in this tissue. To assess the benefit of including an intron *in vivo*, we calculated the average percent contribution of each promoter (via the 3 bp barcode) among all regions from both NHPs and divided it by the percent of that same promoter in the input virus ([Figure 3C](#)). This normalized output showed an intron length-dependent enhancement in transcription for some promoters (*CD42A*, *ANXA1*, and *OGFRL1*), no benefit for others (*ANXA2* and *FOS*), and a detriment for *VWA3A*. Despite this unexpected output, all *VWA3A* variants showed higher enrichment than any other promoter variant. Given the consistent, relatively strong use of the *VWA3A* promoter *in vivo* and knowledge that IME can function at both the transcriptional and translational levels, we chose the *VWA3A* short intron promoter for downstream experiments ([Figures 3C](#) and [S1C](#)).

Validation of cross-species function of human *VWA3A* promoter in mice

In our initial screen using human-derived promoter sequences in mice, *VWA3A* showed relative enrichment over the input virus, suggesting productive promoter use across species ([Figure 2D](#)). To validate expression and localization, AAV4.VWA3A.eGFP was injected into the lateral ventricle of adult WT mice. After 4 weeks, a strong eGFP signal was detected in the ependyma and choroid plexus ([Figure 4A](#)). We next tested if the *VWA3A* promoter could drive high ependymal expression and detectable levels of secreted ApoE2 protein in mice CSF. AAV4.iCAG.APOE2 or AAV4.VWA3A short intron.APOE2 vector was injected into the anterior lateral ventricle of adult ApoE null (ApoE^{-/-}) mice at a dose of 6E9 vg ([Figure 4B](#)).

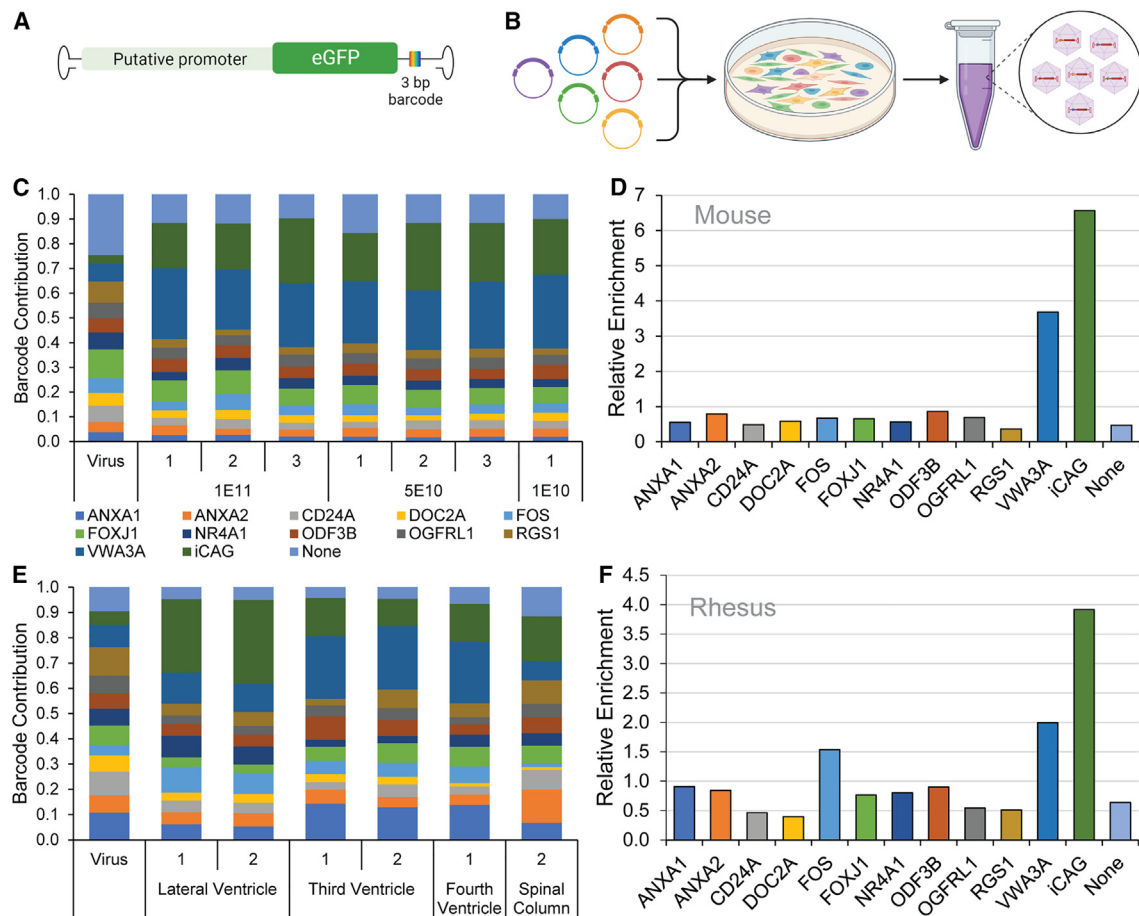


Figure 2. Library screening of human-derived ependyma promoters in mouse and rhesus

(A) Human sequence-derived promoter regions (up to 3 kb) were appended upstream of an eGFP reporter. For library screening, a unique 3 bp barcode was added to the 3' UTR. (B) Individual plasmids were pooled at equimolar concentrations and transfected as a library into HEK293 cells for packaging into a single virus (AAV2 for rhesus or AAV4 for mouse). (C) Fractional read counts associated with each promoter (barcode) in mouse ependyma and input AAV4 library. Only one sample treated with 1E10 vg showed sufficient barcode recovery. (D) Relative enrichment calculated by normalizing the fractional promoter output (RNA reads) to the fractional input (Virus DNA). (E) Fractional read counts associated with each promoter in rhesus ependyma. Numbers 1 and 2 indicate two different rhesus macaques. Missing samples reflect an inability to recover RNA barcodes. (F) Same as in (D) for rhesus.

After 4 weeks, CSF was collected and APOE was detected by automated western blot (Figure 4C). APOE levels in CSF from mice injected with AAV4.VWA3A short intron.APOE2 were 2–12× higher than in CSF from AAV4 expressing-APOE2 from the iCAG-promoter (Figure 4D).

DISCUSSION

Widespread AAV delivery in the CNS can be achieved by systemic delivery of BBB-penetrating capsids or direct delivery to the CSF. For expression of secreted proteins, direct CSF delivery of ependyma-tropic capsids enables localized protein production and broad distribution via CSF flow through the ventricular, subarachnoid, and perivascular spaces. Here we improved upon this approach by identifying an ependyma-specific promoter to de-target direct neuronal expression and drive strong transcription and protein secretion into the CSF.

The ependyma comprises a single layer of simple columnar epithelial cells and forms a physical boundary between the CSF and surrounding CNS parenchyma. These ciliated cells play critical roles in CSF homeostasis and removal of waste from the brain. Extensive single cell^{36–38} and bulk RNA analysis on sorted cells³⁹ has identified over 400 ependyma-enriched genes relative to those in the adjacent subependymal/subventricular zone. One limitation to using these analyses is their derivation from healthy animals or human tissue while neurodegenerative diseases including AD and Huntington's disease may exhibit ependymal dysfunction.⁴⁰ Our study included human brain samples that spanned multiple neurodegenerative diseases and a 50-year window of adult aging (Table 1), enabling identification of robust gene signatures for therapeutic or discovery applications.

Cell-type-specific transcript identification from bulk tissue RNA has been historically achieved using cDNA subtraction libraries.⁴¹ Here,

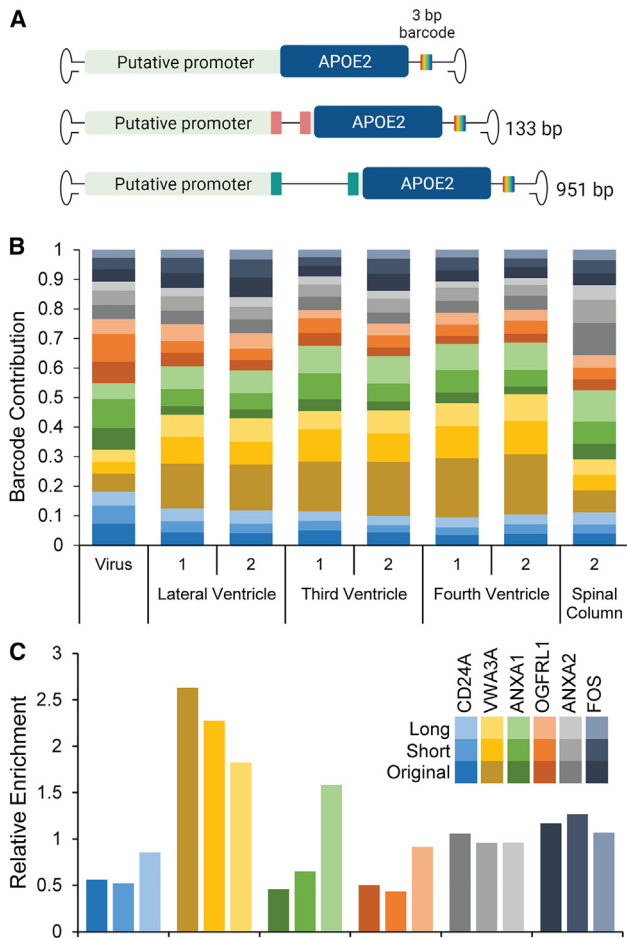


Figure 3. Addition of introns differentially affects transgene transcription
 (A) Maps depicting the three different no intron-, short intron-, and long intron-containing promoter variants. (B) Fractional contribution of transgene-related barcodes in RNA isolated from rhesus ependyma and input virus. (C) Relative promoter enrichment calculated as the fractional contribution in recovered RNA relative to that in the input virus.

we took a similar approach, comparing adjacent tissue samples with and without our cell type of interest and performed computational, rather than physical, subtraction. Our approach proved successful in identifying specific genes, with 37 of the top 90 having been previously associated with ependyma.^{36–38} Among these genes was *FOXJ1*, a commonly used marker of ependyma whose promoter has been used experimentally to drive localized expression.⁴² GO analysis of uncharacterized hits identified axoneme and ciliary plasm as top cellular component categories, further expanding our list of tissue-associated genes (Table S1).

In translating our top hits into promoters, our definition of “promoter” extended far beyond typical eukaryotic promoter lengths of 100–1,000 bp, allowing inclusion of up to 3,000 bp of transcript-adjacent sequence. These promoter lengths helped ensure inclusion of functional elements and were suitable for expressing short transgenes.

Given this over-estimation in initial length, significant truncations capable of driving expression can likely be generated to accommodate larger transgenes.

By incorporation and comparison of transcript-associated 3 bp barcodes we were able to directly compare transcriptional activity of pooled ependyma-specific promoters in the same animal. Using our promoter-less variant (None) as a negative control, nearly all human sequences drove some transcriptional activity over baseline in both mouse and rhesus tissue (Figures 2D and 2F). Our screens found transcript abundance from our human *VWA3A*-derived sequence to be approximately half from the ubiquitous iCAG promoter. The specificity of this promoter for ependyma expression in brain is supported by published ISH data (Allen Brain Atlas), single-cell enrichment of the *VWA3A* gene,³⁸ and recent inclusion in a set of cilia-associated genes.⁴³ Surprisingly, *FOXJ1* did not show strong enrichment despite significant sequence overlap with a previously defined *FOXJ1* promoter.⁴⁴ While trends in promoter use were largely concordant among brain and spinal cord, spinal cord samples from NHPs revealed unique enrichment of *ANXA2* (Figures 2E and 3B) perhaps reflecting differential identity of ependymal cells lining the spinal column.⁴⁵

In a follow-on NHP screen, we tested the ability for a transgene-localized intron to increase expression via IME. Preliminary screening of transfected HEK293 cells supported increased protein output from intron-containing transgenes with a positive length relationship (Figure S1); however, this relationship was not consistently observed at the transcript level *in vivo* (Figure 3C). IME can affect both transcription and translation, and our discordant results may reflect measurement at two different stages of expression.⁴⁶

Individual promoter validation was initially tested using mouse sequences in mouse tissue using AAV4. All promoter segments tested resulted in efficient eGFP expression in ependymal cells demonstrating sensitivity (Figure 3D); however, the narrow tropism of i.c.v.-delivered AAV4 to the ependyma limited assessment of sequence specificity.^{29,47} This same limitation exists for AAV2 in dogs²⁶ and NHPs where transduction is also confined to the ependyma (B.L.D., unpublished data). Tissue-specific transcription will require experimental validation following CSF delivery with more broadly tropic capsids such as AAV7 or AAV9.⁴⁸

When delivered using the ependyma-specific capsid AAV4, our *VWA3A* promoter showed an expression advantage, driving higher APOE protein secretion into the CSF compared with an iCAG control (Figure 4C). This finding contrasted with predictions from our initial screen of human promoters in mouse where iCAG showed the greatest enrichment (Figures 2D and 2F), further supporting IME of translation.⁴⁶

In summary, we have identified a promoter for ependyma-derived transgene expression. This promoter, derived from the *VWA3A* gene, is predicted to maintain activity in settings of disease and aging and is capable of driving transcription in both mouse and NHP tissue.

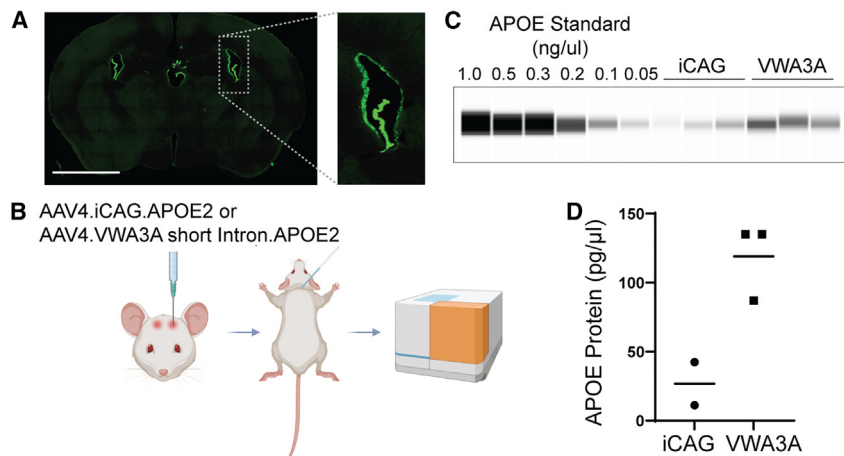


Figure 4. Human VWA3A promoter drives expression in mouse ependyma and protein secretion into the CSF

(A) Coronal section of a mouse brain injected i.c.v. with 2.7E10 total viral genomes AAV4.VWA3A.eGFP vector. Zoom region outlines ependymal transduction in the lateral ventricle. Scale bar, 2.5 mm. (B) Experimental paradigm to measure transgene-derived APOE2 in the CSF of ApoE^{-/-} mice. (C) Wes analysis and (D) quantification of vector-derived APOE2 in CSF of ApoE^{-/-} mice. The first iCAG sample lay outside our standard curve and was not quantified. Bars represent group mean.

Furthermore, transgene expression downstream of the VWA3A promoter resulted in higher protein secretion than a strong ubiquitous iCAG promoter, supporting its use for therapeutic and research applications.

MATERIALS AND METHODS

Study approval and animal housing

Mice were housed in a climate-controlled environment and kept on a 12 h light/dark cycle with access to food *ad libitum*. Library groups were age matched and included approximately equal numbers of male and female mice.

A total of three male and one female rhesus macaques were used in this study and were aged between 3 and 6 years. All NHPs were screened for relevant neutralizing antibodies against the parental AAV serotypes before enrollment and tested negative. Physical exams were performed by a veterinarian trained in NHP medicine. Rhesus macaques were captive-born and socially housed while on study. NHPs were exposed to a 12 h light/dark cycle, offered *ad libitum* access to reverse-osmosis purified water and fed twice daily with portions of Purina LabDiet Certified Primate Diet (5048) supplemented with fresh fruits and vegetables as part of their behavioral enrichment program. This study was conducted in accordance with the Guide for the Care and Use of Laboratory Animals (National Research Council) and the Animal Welfare Act of 1966 (P.L. 89-544), as amended.

All animals were housed at the CHOP Research Institute (RI). All procedures were approved by the CHOP RI Institutional Animal Care and Use Committee. The CHOP RI is fully accredited by AAALAC International.

Human autopsy tissue collection

Human brain tissue was obtained from the Massachusetts Alzheimer Disease Research Center Tissue Bank. Tissue was dissected at the time of autopsy and immediately snap frozen with powdered dry ice. Post-mortem intervals were less than 24 h. Each patient sample was obtained from slabs at the level of the caudate and was comprised of

paired white matter and/or gray matter samples, with one of each pair overlapping the ventricle margin and the other in adjacent parenchyma. All sample collection was obtained under a research protocol approved by the Massachusetts General Hospital IRB.

RNA isolation and library preparation

Total RNA was extracted from fresh human autopsy samples using mirVana miRNA isolation kit (Thermo Fisher Scientific). RNA integrity (RIN) was measured using an Agilent Bioanalyzer. Samples with RIN > 6 were included for sequencing. Libraries were prepared with the Illumina TruSeq Stranded mRNA Library Prep kit according to manufacturer's protocol (Illumina) by the University of Iowa Institute of Human Genetics.

RNA from micro-dissected mouse and rhesus macaque ependyma was isolated using TRIzol according to the manufacturer's instructions (Invitrogen). Samples were DNase treated using TURBO DNase and reverse transcribed with MultiScribe RT (Applied Biosystems). A sequencing template was generated using two rounds of PCR. First round primers (Table S2) amplified the region immediately surrounding the 3' UTR-localized 3 bp barcode, incorporating a unique molecular identifier (UMI) for PCR collapse and complementary overhangs for the second PCR. Second round primers appended i5 and i7 Illumina adapters for sequencing.

RNA sequencing and analysis

Human autopsy libraries were sequenced on two lanes of a HiSeq4000 with 150 bp paired-end chemistry with an average 14 million read pairs per sample. Fastq files were aligned to the human hg38 reference genome and gene expression was quantified using rsem-calculate-expression 1.3.8 and STAR aligner (v.2.5.2b). Quality metrics were determined using qualimap v.2.2.1. Matrices comparing samples with and without ependyma in Control and Disease groups were generated using rsem-generate-data-matrix and differential expression was calculated using EBSeq. Ependyma-enriched genes from both groups were intersected to identify a list of promoter candidates. Genes with a mean expression value equal to 0 in either group and/or a fold change (Disease/Control) < 0.5 were excluded. Human genes lacking a mouse ortholog were also excluded. Our final list was ranked

by average expression in the Disease group and final library selections were based on manual validation of ependyma-localized expression in the Allen Brain Atlas.

Promoter libraries were prepared for Illumina sequencing using nested PCR described above and sequenced on a single lane of an Illumina HiSeq 4000 flow cell. The resulting fastq files were processed using a custom python script to extract and count 3mer DNA barcodes and 10mer UMI sequences. A custom R script was used to consolidate DNA barcode and UMI counts from each sample, outputting UMI collapsed counts from all samples and barcodes in a single table. Percent contribution was then calculated by dividing reads associated with each barcode by the total barcode reads for that sample. Relative enrichment represents promoter use (RNA) relative to template DNA and was calculated by dividing the percent contribution in tissue by the percent contribution of that same promoter in the input virus.

Promoter annotation and vector preparation

Putative promoter sequences were inferred using ENCODE Regulation and predicted *cis*-regulatory element annotations of upstream genes of interest in the UCSC Genome Browser (GRCh38/hg38 or NCBI37/mm9). Up to 3,000 bp was PCR amplified and appended upstream of an eGFP reporter by NEB HiFi Assembly or ligation into an AAV2 proviral vector (Table S2). Offset annealed oligos were prepared to introduce 3 bp barcodes between NheI-NotI in the 3' UTR. A short chimeric intron from human β -globin and immunoglobulin heavy chain genes or a long chimeric intron from chicken β -actin and rabbit β -globin genes were PCR amplified and inserted near the 3' end of the promoters, downstream of predicted transcription start sites. As the amplified ANXA1 promoter region contained an endogenous partial intron sequence, a 3' segment of each intron was appended to approximate the length of the two introns (total length: short 348 bp; long 901 bp).

For library preparation, plasmids were pooled at equimolar concentrations. Recombinant AAV serotype AAV2/4 (mouse) or AAV2/2 (rhesus) vectors were generated at the Children's Hospital of Philadelphia Research Vector Core and resuspended in Diluent Buffer (Research Vector Core). Vector titers were determined by quantitative PCR using primers targeting the eGFP (Table S2) or ApoE (Hs00171168_m1) transgene.

Vector administration and tissue isolation

WT FVB/NJ (strain: 001800) and ApoE null (ApoE^{-/-}) (strain: 002052) mice were obtained from Jackson Laboratory. Vectors were injected unilaterally into the anterior lateral ventricle (coordinates: +0.86 mm rostral to bregma, \pm 1.8 mm from midline, and -3.5 mm deep from skull). Single mouse promoter vectors were delivered at varying doses (eGFP: *Vwa3a* 2.9E10, *FoxJ1* 4.5E10, *Odf3b* and CMV 6.4E10, *VWA3a* 2.7E10, or ApoE2: iCAG and *VWA3a*.shortInt 6E9 total viral genomes) determined by production titer. AAV4 libraries were delivered at 1E10, 5E10, or 1E11 total viral genomes.

NHP vector delivery followed previously published procedures.⁴⁹ In brief, infusion trajectories were determined on a 3 T research MRI unit (Siemens Trio; SYNGO Vb17) using T1-weighted 3D MPRAGE sequences. To confirm intraventricular placement of the needle tip, 5 μ L of radiographic contrast (ISOVUE-M, Bracco Imaging) was injected under fluoroscopic guidance (OEC 9900 Elite, GE Healthcare) using a micro-infusion pump (Harvard Apparatus PHD Ultra, Harvard Apparatus). After verification, 2E13 or 2.8E13 total viral genomes were delivered in a total infusion volume of 4 mL at a rate of 0.1 mL/min followed by a 10 min dwell. Post infusion, bone wax occluded the trephine and the incision was sutured closed and infiltrated with a local anesthetic. The animals were removed from the stereotactic frame and allowed to recover in a separate cage and isolated from peers until they were able to sit upright without support. Animals were returned to their regular housing configuration once fully recovered from anesthesia, as determined by study staff. Analgesic coverage was provided for a minimum period of 72 h and animals were monitored daily throughout the study.

For visualization of eGFP, mice were anesthetized with 2.5% isoflurane/oxygen mixtures and transcardially perfused with 4% paraformaldehyde (PFA). Tissues were post-fixed overnight in 4% PFA before transfer to 30% sucrose for 48 h. Tissue sections (40 μ m) were cut using a microtome and mounted for direct eGFP visualization using a Leica DM6000B microscope. After 4 weeks, mice injected with the AAV4 library were anesthetized with ketamine/xylazine and transcardially perfused with ice-cold phosphate-buffered saline (PBS). The entire brain was removed and transferred to ice-cold PBS to chill. Three, 2 mm coronal sections were cut using a brain matrix and used for ependyma micro-dissection. Tissue segments were transferred immediately to chilled TRIzol and stored at -80°C until use.

Three or 4 weeks following injection, NHPs were fasted overnight, sedated, intubated, and anesthetized using isoflurane. Upon confirmation of deep anesthesia (stage III, plane 3), we performed a thoracotomy and cardiac perfusion with ice-cold PBS. Brains were removed and chilled and then cut into 4 mm thick coronal slabs. Ependyma was manually micro-dissected from the ventricle margins, snap frozen in liquid nitrogen, and stored at -80°C until further processing.

CSF collection and analysis

Intracisternal CSF collections from mice were performed under general anesthesia with isoflurane. Animals were positioned ventral side down and the neck was flexed for easier access to the cisterna magna. A longitudinal incision was made in the neck skin and cervical muscles were laterally separated until the cisterna magna was available. A pulled borosilicate glass capillary (World Precision Instruments) was inserted through the membrane and CSF was collected by capillarity. Collected CSF was snap frozen with dry ice and kept at -80°C until analysis.

ApoE levels in CSF were quantified using a Wes Simple Western-blot system (Protein Simple, Bio-technique) and Compass software (Protein

Simple) following the manufacturer's indications. In brief, a six point standard curve from 0.05 to 1 ng/μL protein was produced with human recombinant ApoE2 (Pepro Tech, no. 350-12) diluted with 0.1× sample buffer (Protein Simple, no. 042-195). CSF samples and standard curve points were combined with 5× Fluorescent Master Mix at 4:1 ratio, denatured at 95°C for 5 min, spun down at 4°C, and then loaded into a 12–230 kDa separation capillary cartridge (Protein Simple, no. SM-W004). A ratio of 1:50 rabbit anti-human ApoE polyclonal antibody (Novus, no. NBP1-31123) and anti-rabbit detection module (Protein Simple, no. DM-001) was used for ApoE detection.

DATA AVAILABILITY

Data will be made available upon publication according to CHOP policies.

SUPPLEMENTAL INFORMATION

Supplemental information can be found online at <https://doi.org/10.1016/j.omtn.2023.07.016>.

ACKNOWLEDGMENTS

This work was supported by NIH grants P30 AG062421-05 (B.T.H.) and NS111671 (B.L.D.) and by the CHOP Research Institute. Figures and graphical abstract were created with [BioRender.com](https://www.biorender.com).

AUTHOR CONTRIBUTIONS

E.M.C., Y.H.C., P.T.R., L.N.S., L.T., B.T.H., and B.L.D. designed the experiments, analyzed the data, and wrote the manuscript with input and editing from S.L.C., E.H., and M.S.K. Experiments were conducted by E.M.C., Y.H.C., L.T., M.S.K., and E.H.

DECLARATION OF INTERESTS

B.L.D. serves an advisory role with equity in Latus Biosciences, Patch Bio, Voyager Therapeutics, Carbon Biosciences, Spirovant Biosciences, Resilience, Panorama Medicines, Saliogen, and Homology Medicines. She has sponsored research from Novartis, Roche, Latus, Homology Medicines, Saliogen, and Spirovant. B.T.H. is on the scientific advisory board of Latus Bio and has an equity interest. He has a family member who works at Novartis and owns stock in Novartis; he serves on the SAB of Dewpoint and owns stock. He serves on a scientific advisory board or is a consultant for AbbVie, Aprinoia Therapeutics, Arvinas, AvroBio, Axial, Biogen, BMS, Cure Alz Fund, Cell Signaling, Dewpoint, Eisai, Genentech, Ionis, Latus, Novartis, Sangamo, Sanofi, Seer, Takeda, the US Department of Justice, Vigil, and Voyager.

REFERENCES

- Gray, S.J., Foti, S.B., Schwartz, J.W., Bachaboina, L., Taylor-Blake, B., Coleman, J., Ehlers, M.D., Zylka, M.J., McCown, T.J., and Samulski, R.J. (2011). Optimizing promoters for recombinant adeno-associated virus-mediated gene expression in the peripheral and central nervous system using self-complementary vectors. *Hum. Gene Ther.* 22, 1143–1153.
- de Leeuw, C.N., Dyka, F.M., Boye, S.L., Laprise, S., Zhou, M., Chou, A.Y., Borretta, L., McInerney, S.C., Banks, K.G., Portales-Casamar, E., et al. (2014). Targeted CNS Delivery Using Human MiniPromoters and Demonstrated Compatibility with Adeno-Associated Viral Vectors. *Mol. Ther. Methods Clin. Dev.* 1, 5.
- de Leeuw, C.N., Korecki, A.J., Berry, G.E., Hickmott, J.W., Lam, S.L., Lengyel, T.C., Bonaguro, R.J., Borretta, L.J., Chopra, V., Chou, A.Y., et al. (2016). rAAV-compatible MiniPromoters for restricted expression in the brain and eye. *Mol. Brain* 9, 52.
- Shima, Y., Sugino, K., Hempel, C.M., Shima, M., Taneja, P., Bullis, J.B., Mehta, S., Lois, C., and Nelson, S.B. (2016). A Mammalian enhancer trap resource for discovering and manipulating neuronal cell types. *Elife* 5, e13503.
- Graybuck, L.T., Daigle, T.L., Sedeño-Cortés, A.E., Walker, M., Kalmbach, B., Lenz, G.H., Morin, E., Nguyen, T.N., Garren, E., Bendrick, J.L., et al. (2021). Enhancer viruses for combinatorial cell-subclass-specific labeling. *Neuron* 109, 1449–1464.e13.
- Mich, J.K., Graybuck, L.T., Hess, E.E., Mahoney, J.T., Kojima, Y., Ding, Y., Somasundaram, S., Miller, J.A., Kalmbach, B.E., Radaelli, C., et al. (2021). Functional enhancer elements drive subclass-selective expression from mouse to primate neocortex. *Cell Rep.* 34, 108754.
- Vormstein-Schneider, D., Lin, J.D., Pelkey, K.A., Chittajallu, R., Guo, B., Arias-García, M.A., Allaway, K., Sakopoulos, S., Schneider, G., Stevenson, O., et al. (2020). Viral manipulation of functionally distinct interneurons in mice, non-human primates and humans. *Nat. Neurosci.* 23, 1629–1636.
- Hordeaux, J., Buza, E.L., Jeffrey, B., Song, C., Jahan, T., Yuan, Y., Zhu, Y., Bell, P., Li, M., Chichester, J.A., et al. (2020). MicroRNA-mediated inhibition of transgene expression reduces dorsal root ganglion toxicity by AAV vectors in primates. *Sci. Transl. Med.* 12, eaba9188.
- Keaveney, M.K., Tseng, H.A., Ta, T.L., Gritton, H.J., Man, H.Y., and Han, X. (2018). A MicroRNA-Based Gene-Targeting Tool for Virally Labeling Interneurons in the Rodent Cortex. *Cell Rep.* 24, 294–303.
- Odom, D.T., Dowell, R.D., Jacobsen, E.S., Gordon, W., Danford, T.W., MacIsaac, K.D., Rolfe, P.A., Conboy, C.M., Gifford, D.K., and Fraenkel, E. (2007). Tissue-specific transcriptional regulation has diverged significantly between human and mouse. *Nat. Genet.* 39, 730–732.
- Foust, K.D., Nurre, E., Montgomery, C.L., Hernandez, A., Chan, C.M., and Kaspar, B.K. (2009). Intravascular AAV9 preferentially targets neonatal neurons and adult astrocytes. *Nat. Biotechnol.* 27, 59–65.
- Chan, K.Y., Jang, M.J., Yoo, B.B., Greenbaum, A., Ravi, N., Wu, W.L., Sánchez-Guardado, L., Lois, C., Mazmanian, S.K., Deverman, B.E., and Gradinaru, V. (2017). Engineered AAVs for efficient noninvasive gene delivery to the central and peripheral nervous systems. *Nat. Neurosci.* 20, 1172–1179.
- Hordeaux, J., Wang, Q., Katz, N., Buza, E.L., Bell, P., and Wilson, J.M. (2018). The Neurotropic Properties of AAV-PHP.B Are Limited to C57BL/6J Mice. *Mol. Ther.* 26, 664–668.
- Mathiesen, S.N., Lock, J.L., Schoderboeck, L., Abraham, W.C., and Hughes, S.M. (2020). CNS Transduction Benefits of AAV-PHP.eB over AAV9 Are Dependent on Administration Route and Mouse Strain. *Mol. Ther. Methods Clin. Dev.* 19, 447–458.
- Goertsen, D., Flytzanis, N.C., Goeden, N., Chuapoco, M.R., Cummins, A., Chen, Y., Fan, Y., Zhang, Q., Sharma, J., Duan, Y., et al. (2022). AAV capsid variants with brain-wide transgene expression and decreased liver targeting after intravenous delivery in mouse and marmoset. *Nat. Neurosci.* 25, 106–115.
- Stanton, A.C., Lagerborg, K.A., Tellez, L., Krunnusz, A., King, E.M., Ye, S., Solomon, I.H., Tabebordbar, M., and Sabeti, P.C. (2023). Systemic administration of novel engineered AAV capsids facilitates enhanced transgene expression in the macaque CNS. *Méd.* 4, 31–50.e8.
- Bailey, R.M., Rozenberg, A., and Gray, S.J. (2020). Comparison of high-dose intracisterna magna and lumbar puncture intrathecal delivery of AAV9 in mice to treat neuropathies. *Brain Res.* 1739, 146832.
- Hinderer, C., Bell, P., Vite, C.H., Louboutin, J.P., Grant, R., Bote, E., Yu, H., Pukenas, B., Hurst, R., and Wilson, J.M. (2014). Widespread gene transfer in the central nervous system of cynomolgus macaques following delivery of AAV9 into the cisterna magna. *Mol. Ther. Methods Clin. Dev.* 1, 14051.
- Gray, S.J., Nagabhushan Kalburgi, S., McCown, T.J., and Jude Samulski, R. (2013). Global CNS gene delivery and evasion of anti-AAV-neutralizing antibodies by intrathecal AAV administration in non-human primates. *Gene Ther.* 20, 450–459.
- Hinderer, C., Bell, P., Katz, N., Vite, C.H., Louboutin, J.P., Bote, E., Yu, H., Zhu, Y., Casal, M.L., Bagel, J., et al. (2018). Evaluation of Intrathecal Routes of Administration for Adeno-Associated Viral Vectors in Large Animals. *Hum. Gene Ther.* 29, 15–24.

21. Rosenberg, J.B., Kaplitt, M.G., De, B.P., Chen, A., Flagiello, T., Salami, C., Pey, E., Zhao, L., Ricart Arbona, R.J., Monette, S., et al. (2018). AAVrh.10-Mediated APOE2 Central Nervous System Gene Therapy for APOE4-Associated Alzheimer's Disease. *Hum. Gene Ther. Clin. Dev.* 29, 24–47.
22. Hordeaux, J., Buza, E.L., Dyer, C., Goode, T., Mitchell, T.W., Richman, L., Denton, N., Hinderer, C., Katz, N., Schmid, R., et al. (2020). Adeno-Associated Virus-Induced Dorsal Root Ganglion Pathology. *Hum. Gene Ther.* 31, 808–818.
23. Hordeaux, J., Hinderer, C., Goode, T., Katz, N., Buza, E.L., Bell, P., Calcedo, R., Richman, L.K., and Wilson, J.M. (2018). Toxicology Study of Intra-Cisterna Magna Adeno-Associated Virus 9 Expressing Human Alpha-L-Iduronidase in Rhesus Macaques. *Mol. Ther. Methods Clin. Dev.* 10, 79–88.
24. Hordeaux, J., Hinderer, C., Goode, T., Buza, E.L., Bell, P., Calcedo, R., Richman, L.K., and Wilson, J.M. (2018). Toxicology Study of Intra-Cisterna Magna Adeno-Associated Virus 9 Expressing Iduronate-2-Sulfatase in Rhesus Macaques. *Mol. Ther. Methods Clin. Dev.* 10, 68–78.
25. Yamazaki, Y., Hirai, Y., Miyake, K., and Shimada, T. (2014). Targeted gene transfer into ependymal cells through intraventricular injection of AAV1 vector and long-term enzyme replacement via the CSF. *Sci. Rep.* 4, 5506.
26. Katz, M.L., Tecedor, L., Chen, Y., Williamson, B.G., Lysenko, E., Winger, F.A., Young, W.M., Johnson, G.C., Whiting, R.E.H., Coates, J.R., and Davidson, B.L. (2015). AAV gene transfer delays disease onset in a TPP1-deficient canine model of the late infantile form of Batten disease. *Sci. Transl. Med.* 7, 313ra180.
27. Liu, G., Martins, I., Wemmie, J.A., Chiorini, J.A., and Davidson, B.L. (2005). Functional correction of CNS phenotypes in a lysosomal storage disease model using adeno-associated virus type 4 vectors. *J. Neurosci.* 25, 9321–9327.
28. Watson, D.J., Passini, M.A., and Wolfe, J.H. (2005). Transduction of the choroid plexus and ependyma in neonatal mouse brain by vesicular stomatitis virus glycoprotein-pseudotyped lentivirus and adeno-associated virus type 5 vectors. *Hum. Gene Ther.* 16, 49–56.
29. Liu, G., Martins, I.H., Chiorini, J.A., and Davidson, B.L. (2005). Adeno-associated virus type 4 (AAV4) targets ependyma and astrocytes in the subventricular zone and RMS. *Gene Ther.* 12, 1503–1508.
30. Dickson, P., McEntee, M., Vogler, C., Le, S., Levy, B., Peinovich, M., Hanson, S., Passage, M., and Kakkis, E. (2007). Intrathecal enzyme replacement therapy: successful treatment of brain disease via the cerebrospinal fluid. *Mol. Genet. Metabol.* 91, 61–68.
31. Ichimura, T., Fraser, P.A., and Cserr, H.F. (1991). Distribution of extracellular tracers in perivascular spaces of the rat brain. *Brain Res.* 545, 103–113.
32. Spassky, N., Merkle, F.T., Flames, N., Tramontin, A.D., Garcia-Verdugo, J.M., and Alvarez-Buylla, A. (2005). Adult ependymal cells are postmitotic and are derived from radial glial cells during embryogenesis. *J. Neurosci.* 25, 10–18.
33. Hudry, E., Dashkoff, J., Roe, A.D., Takeda, S., Koffie, R.M., Hashimoto, T., Scheel, M., Spires-Jones, T., Arbel-Ornath, M., Betensky, R., et al. (2013). Gene transfer of human Apoe isoforms results in differential modulation of amyloid deposition and neurotoxicity in mouse brain. *Sci. Transl. Med.* 5, 212ra161.
34. Brinster, R.L., Allen, J.M., Behringer, R.R., Gelinis, R.E., and Palmiter, R.D. (1988). Introns increase transcriptional efficiency in transgenic mice. *Proc. Natl. Acad. Sci. USA* 85, 836–840.
35. West, H.L., Rebeck, G.W., and Hyman, B.T. (1994). Frequency of the apolipoprotein E epsilon 2 allele is diminished in sporadic Alzheimer disease. *Neurosci. Lett.* 175, 46–48.
36. MacDonald, A., Lu, B., Caron, M., Caporicci-Dinucci, N., Hatrock, D., Petrecca, K., Bourque, G., and Stratton, J.A. (2021). Single Cell Transcriptomics of Ependymal Cells Across Age, Region and Species Reveals Cilia-Related and Metal Ion Regulatory Roles as Major Conserved Ependymal Cell Functions. *Front. Cell. Neurosci.* 15, 703951.
37. Shah, P.T., Stratton, J.A., Stykel, M.G., Abbasi, S., Sharma, S., Mayr, K.A., Koblinger, K., Whelan, P.J., and Biernaskie, J. (2018). Single-Cell Transcriptomics and Fate Mapping of Ependymal Cells Reveals an Absence of Neural Stem Cell Function. *Cell* 173, 1045–1057.e9.
38. Zywitzka, V., Misios, A., Bunatyan, L., Willnow, T.E., and Rajewsky, N. (2018). Single-Cell Transcriptomics Characterizes Cell Types in the Subventricular Zone and Uncovers Molecular Defects Impairing Adult Neurogenesis. *Cell Rep.* 25, 2457–2469.e8.
39. Beckervordersandforth, R., Tripathi, P., Ninkovic, J., Bayam, E., Lepier, A., Stempfhuber, B., Kirchoff, F., Hirrlinger, J., Haslinger, A., Lie, D.C., et al. (2010). In vivo fate mapping and expression analysis reveals molecular hallmarks of prospectively isolated adult neural stem cells. *Cell Stem Cell* 7, 744–758.
40. Nelles, D.G., and Hazrati, L.N. (2022). Ependymal cells and neurodegenerative disease: outcomes of compromised ependymal barrier function. *Brain Commun.* 4, fca288.
41. Klickstein, L.B. (2001). Production of a subtracted cDNA library. *Curr. Protoc. Mol. Biol.* 55, Unit 25B 21.
42. Carlen, M., Meletis, K., Göritz, C., Darsalia, V., Evergren, E., Tanigaki, K., Amendola, M., Barnabé-Heider, F., Yeung, M.S.Y., Naldini, L., et al. (2009). Forebrain ependymal cells are Notch-dependent and generate neuroblasts and astrocytes after stroke. *Nat. Neurosci.* 12, 259–267.
43. Patir, A., Fraser, A.M., Barnett, M.W., McTeir, L., Rainger, J., Davey, M.G., and Freeman, T.C. (2020). The transcriptional signature associated with human motile cilia. *Sci. Rep.* 10, 10814.
44. Zhang, Y., Huang, G., Shornick, L.P., Roswit, W.T., Shipley, J.M., Brody, S.L., and Holtzman, M.J. (2007). A transgenic FOXJ1-Cre system for gene inactivation in ciliated epithelial cells. *Am. J. Respir. Cell Mol. Biol.* 36, 515–519.
45. Alfaro-Cervello, C., Soriano-Navarro, M., Mirzadeh, Z., Alvarez-Buylla, A., and Garcia-Verdugo, J.M. (2012). Biciliated ependymal cell proliferation contributes to spinal cord growth. *J. Comp. Neurol.* 520, 3528–3552.
46. Nott, A., Meislin, S.H., and Moore, M.J. (2003). A quantitative analysis of intron effects on mammalian gene expression. *RNA* 9, 607–617.
47. Davidson, B.L., Stein, C.S., Heth, J.A., Martins, I., Kotin, R.M., Derksen, T.A., Zabner, J., Ghodsi, A., and Chiorini, J.A. (2000). Recombinant adeno-associated virus type 2, 4, and 5 vectors: transduction of variant cell types and regions in the mammalian central nervous system. *Proc. Natl. Acad. Sci. USA* 97, 3428–3432.
48. Samaranch, L., Salegio, E.A., San Sebastian, W., Kells, A.P., Bringas, J.R., Forsayeth, J., and Bankiewicz, K.S. (2013). Strong cortical and spinal cord transduction after AAV7 and AAV9 delivery into the cerebrospinal fluid of nonhuman primates. *Hum. Gene Ther.* 24, 526–532.
49. Ranum, P.T., Tecedor, L., Keiser, M.S., Chen, Y.H., Leib, D.E., Liu, X., and Davidson, B.L. (2023). Cochlear transduction via cerebrospinal fluid delivery of AAV in non-human primates. *Mol. Ther.* 31, 609–612.